*Acta Oceanol. Sin.*, 2019, Vol. 38, No. 11, P. 51–61
https://doi.org/10.1007/s13131-019-1498-z
http://www.hyxb.org.cn
E-mail: hyxbe@263.net

# Significant salinity increase in subsurface waters of the South China Sea during 2016–2017

Xingrong Chen[1], Zenghong Liu[2, 3*], Haiyan Wang[1], Dongfeng Xu[2, 3], Lei Wang[3]

[1] National Marine Environmental Forecasting Center, Beijing 100081, China

[2] State Key Laboratory of Satellite Ocean Environment Dynamics, Ministry of Natural Resources, Hangzhou 310012, China

[3] Second Institute of Oceanography, Ministry of Natural Resources, Hangzhou 310012, China

Received 26 July 2019; accepted 16 August 2019



**Abstract**

The South China Sea (SCS) is the largest semi-enclosed marginal sea in the North Pacific. Salinity changes in the SCS play an important role in regional and global ocean circulation and the hydrological cycle. However, there are few studies on salinity changes over the SCS due to lack of high-quality and long-term observations. In the past decade, the deployment of floats from the Argo program in the SCS and their accumulated temperature and salinity profiles have made it possible for us to examine salinity changes over the entire basin. In this study, salinity changes were investigated with Argo and underwater glider temperature and salinity observations and gridded temperature–salinity objective analyses (UK Met Office Hadley Centre EN4.2.1 objective analysis and China Argo Real-time Data Center BOA_Argo). The results indicated that the subsurface water in the entire SCS became significantly saltier during 2016–2017. The most significant salinity increase was found during 2016 in the northeastern SCS. The subsurface water in the northeastern SCS exhibited a salinity maximum above 35, which was recorded by three Argo floats during 2015–2016. Such high salinity water was rarely observed and reported prior to the Argo era. Average salinity of 2016–2017 along the $25.5\sigma_\theta$–$23.5\sigma_\theta$ isopycnal surfaces in the whole SCS is 0.014–0.130 higher than the climatology. Increases in subsurface salinity started from the northeastern SCS and extended southwestward gradually. Moreover, the subsurface salinity changes, especially in the northern SCS, exhibited a semiannual lead behind the subsurface Luzon Strait transport. Further analysis indicated that the predominance of advection, driven by subsurface Luzon Strait transport, led to salinification along the western boundary of the SCS. In other parts of the SCS, negative wind stress curl trends tended to preserve the high salinity characteristics of the subsurface water.

**Key words:** South China Sea, salinification, subsurface, Luzon Strait transport

**Citation:** Chen Xingrong, Liu Zenghong, Wang Haiyan, Xu Dongfeng, Wang Lei. 2019. Significant salinity increase in subsurface waters of the South China Sea during 2016–2017. Acta Oceanologica Sinica, 38(11): 51–61, doi: 10.1007/s13131-019-1498-z

## 1 Introduction

Ocean salinity is an important parameter in physical oceanography, and changes in it are an indirect indicator for changes in precipitation, evaporation, river runoff, and ice melt. The patterns of salinity change are often used to study changes in the global hydrological cycle (Wong et al., 1999; Curry et al., 2003) and are an important complement to atmospheric measurements. Because of their importance, salinity changes on global and regional scales have been studied extensively (e.g., Wong et al., 1999, 2001; Suga et al., 2000; Lukas, 2001; Jacobs et al., 2002; Curry et al., 2003; Boyer et al., 2005; Delcroix et al., 2007; Durack and Wijffels, 2010).

The South China Sea (SCS) is the largest semi-enclosed marginal sea in the North Pacific. It connects with the Pacific Ocean through the deep Luzon Strait. The Kuroshio intrusion through the Luzon Strait is a year-round phenomenon (Shaw, 1991; Qu et al., 2000, 2004), which affects both the circulation and water characteristics in the SCS. Compared with SCS water in the subsurface, Kuroshio water is characterized by higher temperature and salinity. Over the past decades, much work has focused on the Kuroshio intrusion, water exchange through the Luzon Strait, and circulation in the SCS (e.g., Shaw, 1991; Shaw and Chao, 1994; Li et al., 2000; Qu, 2000; Li and Qu, 2006; Tsui and Wu, 2012; Yuan et al., 2014; Hsin, 2015; Wang et al., 2016). However, less efforts have been exerted to study salinity changes in the SCS due to a lack of high-quality observation data sets. Nan et al. (2013) reported decadal freshening in the northeastern SCS from the 1990s to 2000s because of a weakening of the Kuroshio intrusion. Using sea surface salinity data from the sensor Aquarius sponsored by NASA's Earth System Science Pathfinder (ESSP) Program together with in situ hydrographic data, Zeng et al. (2014) revealed a reliable freshening in the SCS in 2012 owing to abundant local freshwater flux and weakening of the Kuroshio intrusion. Zeng et al. (2016) reported a Pacific Decadal Oscillation (PDO)-like change in the subsurface salinity of the northern SCS over the period 1960–2012, and a long-term freshening of –0.007 8 $a^{-1}$

Foundation item: The National Basic Research Program (973 Program) of China under contract No. 2016YFC0304105; the National Natural Science Foundation of China under contract Nos 41621064, 41606003 and U1811464; the Sino-German cooperation project "The Response of Circulation and Ecosystem of Northwestern South China Shelf Sea to the Anthropogenic and Nature Influences".
*Corresponding author, E-mail: liuzenghong@139.com

between 1993 and 2012. They also attributed this decadal variation to advection driven by the Luzon Strait transport (LST) and entrainment from the mixed layer. Nan et al. (2016) also found a freshening of –0.012 $a^{-1}$ in the upper 100 m of the SCS between 1993 and 2012. They suggested that this freshening was mainly controlled by the weakening of the Kuroshio intrusion, which is closely related to the PDO. A recent study (Zeng et al., 2018) reported a salinification trend in the SCS from late 2012 when the phase of the PDO switched from negative to positive; however, they mainly focused on the sea surface, and thus the nature of the salinification signal in the subsurface is still unknown.

Over the past few years, the Argo program (Argo Science Team, 1998; Riser et al., 2016; Liu et al., 2017) extended its core mission to cover marginal seas and more profiling floats were launched in the SCS. Thanks to the availability of these high-quality hydrological data, temperature and salinity changes over the basin of the SCS can now be examined. The motivation for this study was to reveal recent subsurface salinity changes and possible factors influencing it (e.g., subsurface LST, local wind stress curl) following previous salinity changes in the SCS described by Zeng et al. (2016) and Nan et al. (2016). The data we used are Argo float-derived temperature and salinity observations that covered nearly the whole SCS basin together with other gridded temperature and salinity data sets. Section 2 of this paper describes the data and methodology. Section 3 reports the significant salinity increase in the subsurface layer of the SCS during 2016–2017. Section 4 discusses possible factors controlling the extreme salinification events. Finally, conclusion and discussions are presented in Section 5.

## 2 Data and methodology

### 2.1 *Argo temperature and salinity data*

As the international Argo program expanded to a global mission in 2013, China began to deploy Argo floats in the SCS from 2016 onwards. Prior to this, all of the floats in the SCS were deployed by the United States. During the period 2006–2018, 143 floats were deployed in the SCS, and about 11 468 temperature–salinity (T–S) profiles were obtained, spanning 5°–22°N and 105°–121°E. The data used in this study were downloaded from the Coriolis Argo Global Data Center (ftp://ftp.ifremer.fr/ifremer/argo/), and have been post-processed by the China Argo Real-time Data Center (CARDC) (http://www.argo.org.cn/). For each float, post quality control has been applied visually to screen out erroneous spikes and conductivity sensor drift. Approximately 10 294 T–S profiles from 117 floats have been retained and used for this study (Fig. 1).

### 2.2 *Sea-wing underwater glider temperature and salinity data*

To include as many in situ observations as possible, data from several Sea-wing underwater gliders were also used. The Sea-wing underwater glider was developed by the Shenyang Institute of Automation, Chinese Academy of Sciences (Yu et al., 2011). From 2014 to 2016, 14 Sea-wing gliders were deployed during eight cruises in the northern SCS from which 1 503 temperature and salinity profiles (each profile contains a downcast and upcast) were observed. Each profile was processed and quality controlled, including a thermal lag correction, Argo-equivalent real-time quality control tests and a simple post-processing procedure, using the toolbox developed by CARDC (Liu et al., 2019).

### 2.3 *Gridded temperature and salinity data set*

We used two gridded temperature and salinity data sets in our analysis. The UK Met Office Hadley Centre EN4.2.1 objective analysis is a monthly product with a 1°×1° horizontal resolution. The EN4 data set is based on subsurface ocean temperature and salinity profile data obtained from the WOD09, GTSPP, Argo and ASBO collections (Good et al., 2013). The BOA_Argo data set developed by CARDC is also a monthly product (1°×1° grid). It is based on a refined version of Barnes' method of successive corrections, and uses only Argo data (Li et al., 2017; Lu et al., 2019). Because the Argo array did not have global coverage prior to 2004, BOA_Argo only provides data from 2004 to 2018. To remove the effects of the seasonal cycle, corresponding monthly averaged climatological salinity fields were derived to represent the seasonal cycle. For EN4 data set, the monthly climatology was computed for the period 1981–2010, while for BOA_Argo, its monthly climatology was derived from the whole data set (2004–2018). The salinity anomaly for each Argo float, Sea-wing underwater glider was then obtained by subtracting the monthly averaged salinity field from BOA_Argo because BOA_Argo data set was produced with only Argo temperature and salinity profiles, and underwater gliders have the similar sampling scheme with Argo floats.

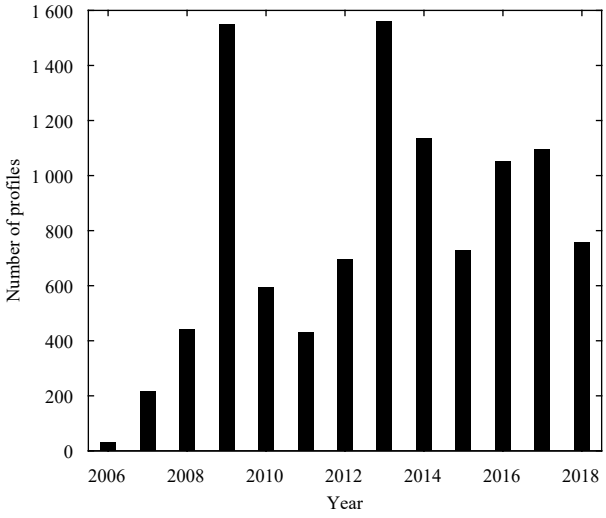


**Fig. 1.** Annual number of Argo temperature–salinity (T–S) profiles from the SCS during the period 2006–2018.

### 2.4 *Ocean current data*

Monthly ocean current data from the National Centers for Environmental Prediction (NCEP) Global Ocean Data Assimilation System (GODAS) (Behringer et al., 1998; Behringer and Xue, 2004) and Simple Ocean Data Assimilation (SODA 3.4.2) ocean/sea ice reanalysis (Carton et al., 2018) were used to calculate the LST into the SCS. The horizontal resolutions of GODAS and SODA 3.4.2 were 1°×0.33° and 0.5°×0.5°, respectively. The calculated LST was used to evaluate the impact of the Kuroshio intrusion on the salinity changes in the SCS.

### 2.5 *Wind data*

The monthly sea surface 10-m wind data used in this study were taken from the NCEP/National Center for Atmospheric Research (NCAR) reanalysis, which has a spatial resolution of 1.875°×1.9° (Kalnay et al., 1996). Similar to EN4 salinity, the ocean current and wind data both subtracted the monthly averaged climatological field for the period 1981–2010 to remove the effects

of the seasonal cycle.

## 3 Significant subsurface salinity increase in the SCS during 2016–2017

The subsurface high-salinity water in the SCS generally exists with a potential density range of $23.5\sigma_\theta$–$25.5\sigma_\theta$ (Qu et al., 2000). We thus used this density range to identify subsurface salinity in the SCS, i.e., the mean salinity value between the $23.5\sigma_\theta$ and $25.5\sigma_\theta$ isopycnal surfaces.

Figure 2 shows a snapshot of observed subsurface salinity anomalies from 2013 to 2018. During 2013–2017, subsurface salinity in the SCS exhibited an increasing trend and reached its peak across the basin between 2016 and 2017. This salinification in the subsurface was weakened starting from 2018 even though there was a remarkable reduction in the total number of the Argo profiles. The salinity increase started in the northern SCS when almost the entire SCS was occupied by a negative salinity anomaly (Figs 2a and b). The most significant salinity increase was found in the northeastern SCS in 2016 and was up to ~0.4 (Fig. 2d). During the Argo era in the SCS, subsurface water with salinity maxima higher than 35 was only observed by three floats (WMO (World Meteorological Organization) numbers: 2901480, 2901502 and 5904562) in the northeastern SCS from 2015 to 2016 (Fig. 3). It is worth noting that such subsurface higher salinity water (>35) has been barely observed and reported in the SCS. This water evidently originated from the western Pacific and intruded into the SCS through the Luzon Strait. All the salinities are found to be consistent with each other below 5°C, indicating the reliability of these Argo observations. The distribution of these profiles may suggest that the intrusion of the Kuroshio water with higher temperature and salinity into the SCS mainly took place in the north of the Luzon Strait, and propagated westward into the SCS from southwest of Taiwan. Furthermore, most profiles (11 out of 13) with salinity maxima higher than 35 were observed throughout 2016. Both the longitude and latitude-time distributions of the subsurface salinity anomalies observed by Argo floats and underwater gliders indicated that the remarkable salinity increases in the subsurface water of the entire SCS was observed in 2016; in addition, the salinity increase seemed to propagate westward and southward (Fig. 4). This southwestward propagation of the positive salinity anomaly was more evident in the EN4 data set (Fig. 5). We excluded data from shallow water (maximum water depth less than 180 m) because of the possibility of unrealistic salinity anomalies. In contrast to 2014, increases in subsurface salinity were most significant in 2016 and 2017, with the maximum anomaly exceeding 0.3 in the northern SCS and southeast of Vietnam. The salinity increase during 2018 was still remarkable, but weakened compared with 2016 and 2017. It can be seen from Fig. 5c that the salinity increase near the Luzon Strait started to decline from 2017, indicating a weakening of the Kuroshio intrusion.

To investigate the spatial distribution of the subsurface salinity changes, we plotted annual mean T–S diagrams for 2016 and 2017 in 3°×3° boxes (Fig. 6). Compared with climatology derived from EN4 data (monthly averaged data for 1981–2010), salinity of the subsurface water showed a remarkable increase across almost the whole basin. Along certain isopycnal surfaces, increases even exceeded 0.2. In fact, almost all the upper ocean above the $25\sigma_\theta$ isopycnal surface in the SCS showed a salinity increase in 2016, especially above the $24.5\sigma_\theta$ isopycnal surface. The upper ocean above the $23.5\sigma_\theta$ isopycnal surface started to freshen in 2017. However, this freshening was absent in the subsurface layers except near the Luzon Strait (Fig. 6b).

The vertical section along 18°N was chosen to illustrate the detailed salinity increasing trend (Fig. 7). During 2015–2018, the salinity increase occurred above ~180 m water depth almost along the entire section compared with 2014. The most signific-

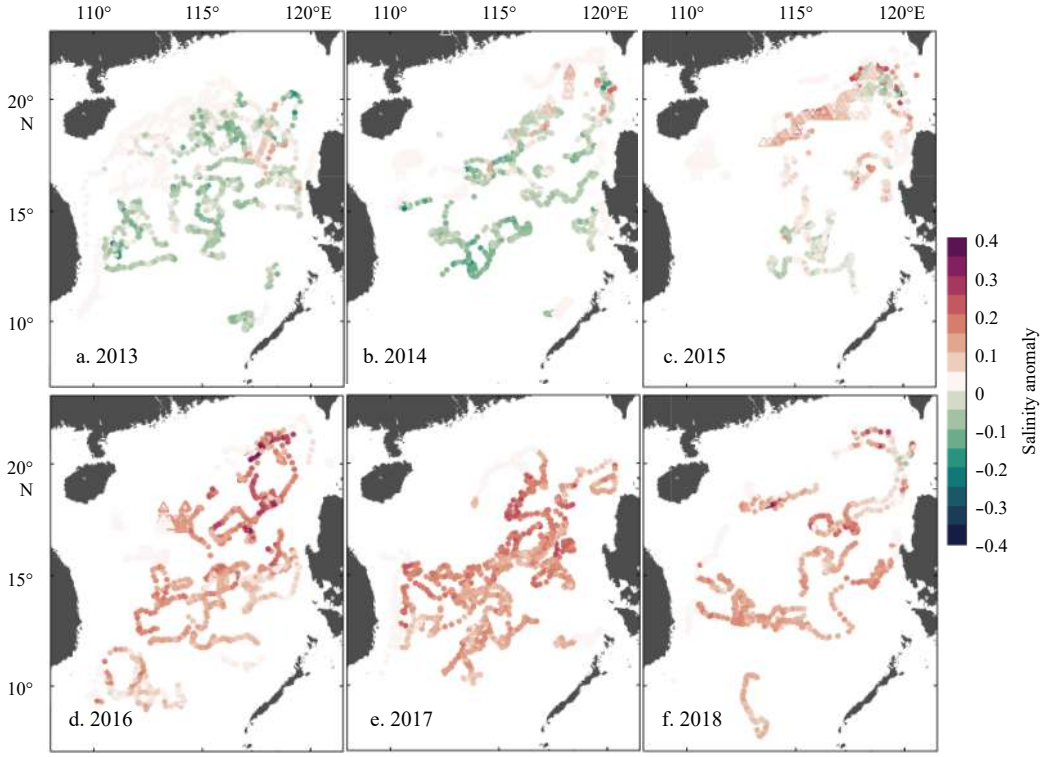


**Fig. 2.** Scatter plots of subsurface salinity anomalies (taken as an average of salinity anomalies within the density range $23.5\sigma_\theta$–$25.5\sigma_\theta$) observed by Argo profiling floats (filled circles) and sea-wing underwater gliders (open triangles) from 2013 to 2018.

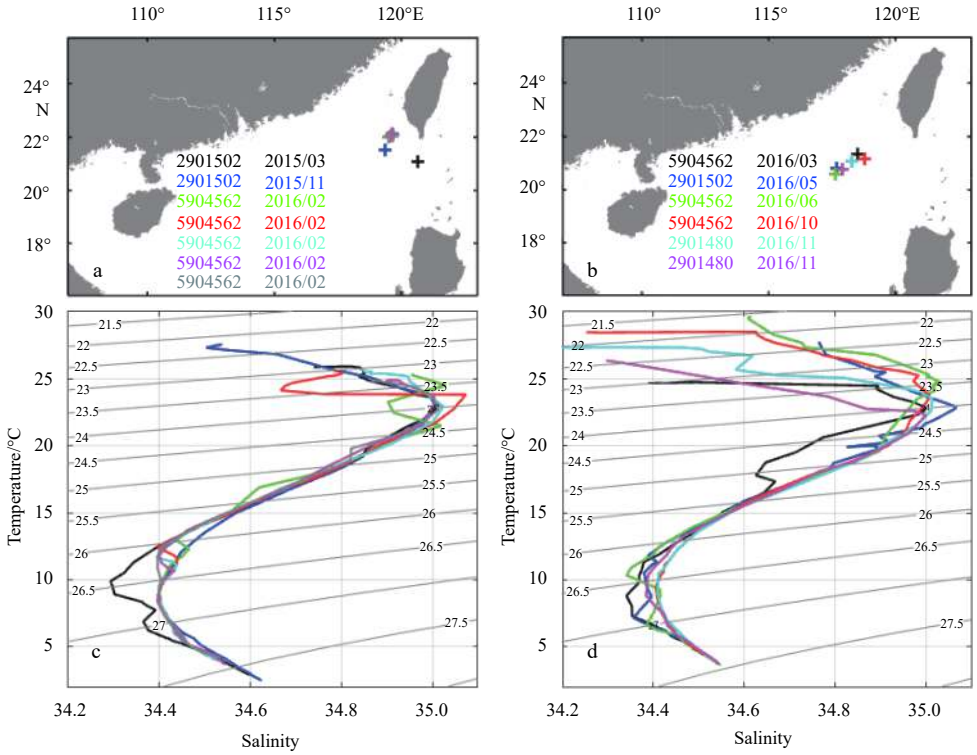


**Fig. 3.** Argo profiles with salinity maxima higher than 35 from 2015 to 2016 in the northeastern SCS. a and b. Profile locations (colored crosses). WMO number and observation date for each profile are superimposed. c and d. T–S curves of Argo profiles shown in (a) and (b), respectively.

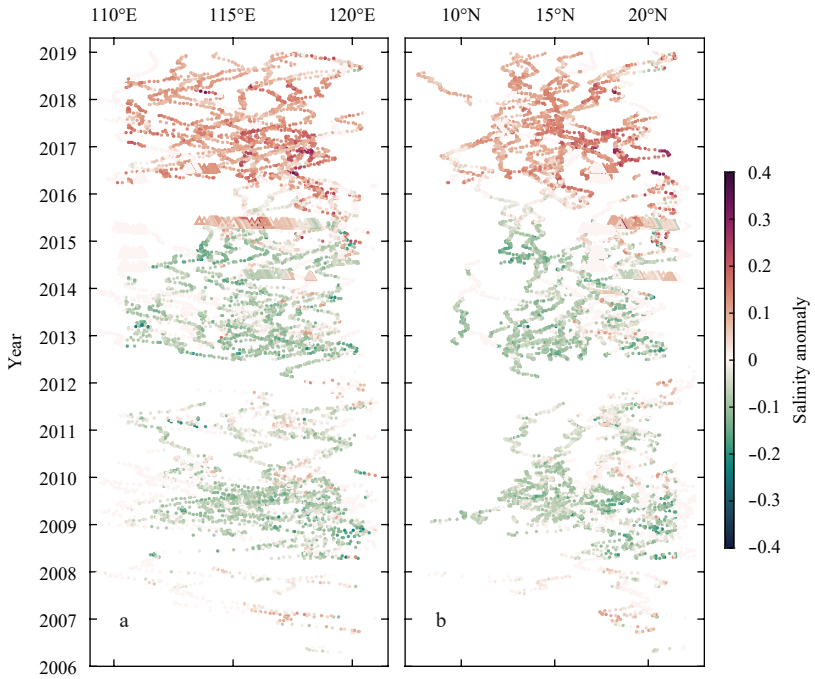


**Fig. 4.** Longitudinal (a) and latitudinal (b) distributions of subsurface salinity anomalies against time observed by Argo floats (filled circles) and sea-wing gliders (open triangles) from 2006 to 2018.

ant salinification trend was located between the sea surface and 24.0$\sigma_\theta$ isopycnal surface, with the maximum exceeding 0.3 during 2016–2017. This positive salinity anomaly reached its highest spatial coverage in 2016, which was in good agreement with observations from Argo floats and Sea-wing gliders. From then on, the salinification trend exhibited a reduction, in particular east of 117°E. During 2015–2018, almost all of the isopycnal contours above 26.0$\sigma_\theta$ were uplifted along 18°N, indicating strengthened upwelling probably as a result of local enhanced wind stress curl. This strengthened isopycnal uplifting was most evident west of

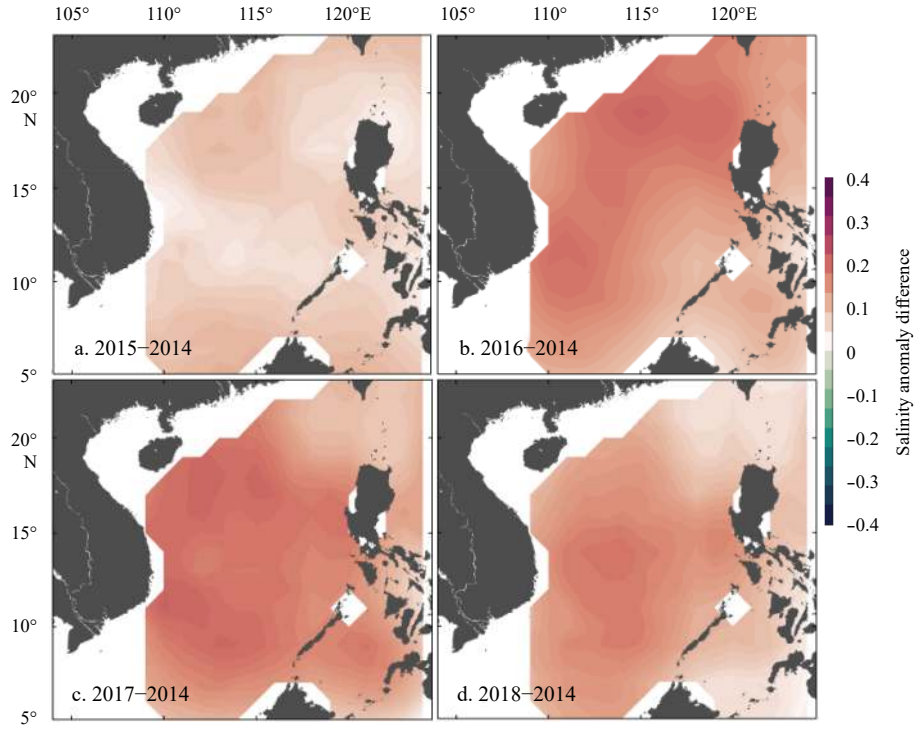


**Fig. 5.** Differences in subsurface salinity anomalies (based on EN4 data) between 2015 and 2014 (a), 2016 and 2014 (b), 2017 and 2014 (c), and 2018 and 2014 (d).

114°E in 2017, with maximum uplifting to ~40 m.

A time series of salinity anomalies from 2004 to 2018 along the 23.5$\sigma_\theta$, 25.0$\sigma_\theta$ and 25.5$\sigma_\theta$ isopycnal surfaces and entire subsurface (23.5$\sigma_\theta$–25.5$\sigma_\theta$) were derived from both EN4 and BOA_Argo data sets to demonstrate a basin-scale view of salinity changes in the subsurface. The recent salinification in the upper ocean of the SCS starting from late 2012 that has been revealed by Zeng et al. (2018) was clearly seen from these two data sets (Fig. 8). This salinification along the 23.5$\sigma_\theta$ and 25.0$\sigma_\theta$ isopycanal surfaces reached its highest during 2016–2017, furthermore, the salinification amplitude along the 23.5$\sigma_\theta$ was much higher than that along the 25$\sigma_\theta$. It seems that the salinity along the 23.5$\sigma_\theta$ has a semiannual leading shift against that along the 25$\sigma_\theta$ isopycnal surface. The salinification along the 23.5$\sigma_\theta$ evidently weakened starting from 2017, which is in good agreement with the Argo-observed freshening in the upper ocean of the SCS shown in Fig. 6b. Both data sets indicated salinification of a similar magnitude along each isopycnal surface, demonstrating that differences in the data sets have minimal effects on salinity change estimates.

Our results also indicated a decadal freshening trend over the basin from 1993 to 2012 (figure not shown), in agreement with Zeng et al. (2016) and Nan et al. (2016); however, an extreme salinification event was found in the SCS subsurface water during 2016–2017 (Fig. 8). The amplitude of this significant salinification in the subsurface water decreased with increasing water density (Table 1). The average salinity anomaly of 2016–2017 in the entire subsurface waters is 0.086 (0.065) for EN4 (BOA_Argo) data set, with the maximum salinification about ~ 0.106 (0.088) in the early of 2017. During the period 2016–2017, EN4 average salinity anomaly is 0.130, 0.063 and 0.014 along the 23.5$\sigma_\theta$, 25.0$\sigma_\theta$ and 25.5$\sigma_\theta$ isopycnal surfaces, respectively. For these same three isopycnal surfaces and period, BOA_Argo average salinity anomaly is 0.119, 0.047 and 0.017, respectively

## 4 Possible factors affecting the subsurface salinity increases during 2016–2017

### 4.1 *Relationship between subsurface salinity changes and subsurface LST*

Significant subsurface salinity increase in the SCS during 2016–2017 are likely to be related to the LST into the SCS, as the Luzon Strait is the only deep channel connecting the SCS with the Pacific Ocean. The advection of the subsurface Luzon Strait transport induces the salinity changes, so the salinity changes in the Luzon Strait (i.e., east of the SCS) can be a good indicator of the subsurface salinity change in the SCS. We calculated the subsurface LST (SLST) across 121°E (between 19.0° and 22.5°N) from the model outputs of GODAS between water depths of 95 m and 205 m at 10-m increments and SODA 3.4.2 between depths of 99 m and 201 m (i.e., 99, 110, 122, 135, 149, 164, 181 and 201 m). The chosen depth ranges almost covered the subsurface layers between 23.5$\sigma_\theta$ and 25.5$\sigma_\theta$ isopycnal surfaces in the SCS and Luzon Strait. Figure 9a shows the time evolution of SLST (with the seasonal cycle removed) calculated from these two data sets for the period 2007–2018. Nan et al. (2013, 2016) reported a weakening of the upper layer LST from the 1990s to 2000s. This weakening also appears in our calculations, and has an annual trend of about $-0.084\times10^6$ and $-0.018\times10^6$ m$^3$/s in the subsurface (not shown) according to GODAS and SODA data, respectively. From 2013 to 2016 (the salinification trend peaked in 2016), a strong yearly positive trend of SLST (as much as $0.538\times10^6$ m$^3$/s from GODAS output) was seen in both data sets, indicating a considerable enhancement of the Kuroshio intrusion (at least in the subsurface) into the SCS in recent years. The LST is closely related to the transport of the North Equatorial Current (NEC), which bifurcates at the Philippines coast into the northward-flowing Kuroshio Current and southward Mindanao Current (Toole et al.,

1990; Qu and Lukas, 2003). Here, we define the NEC bifurcation as the latitude where the meridional velocity averaged within a 5°-longitude band off the continental slope is zero. The subsurface bifurcation latitude of the NEC calculated from both GODAS and SODA clearly tended to shift northward starting from 2013 and reached its northernmost extent in 2016 (Fig. 9b). In late 2012, when the phase of the PDO signal switched from negative to positive (Zeng et al., 2018), the Aleutian low and its related

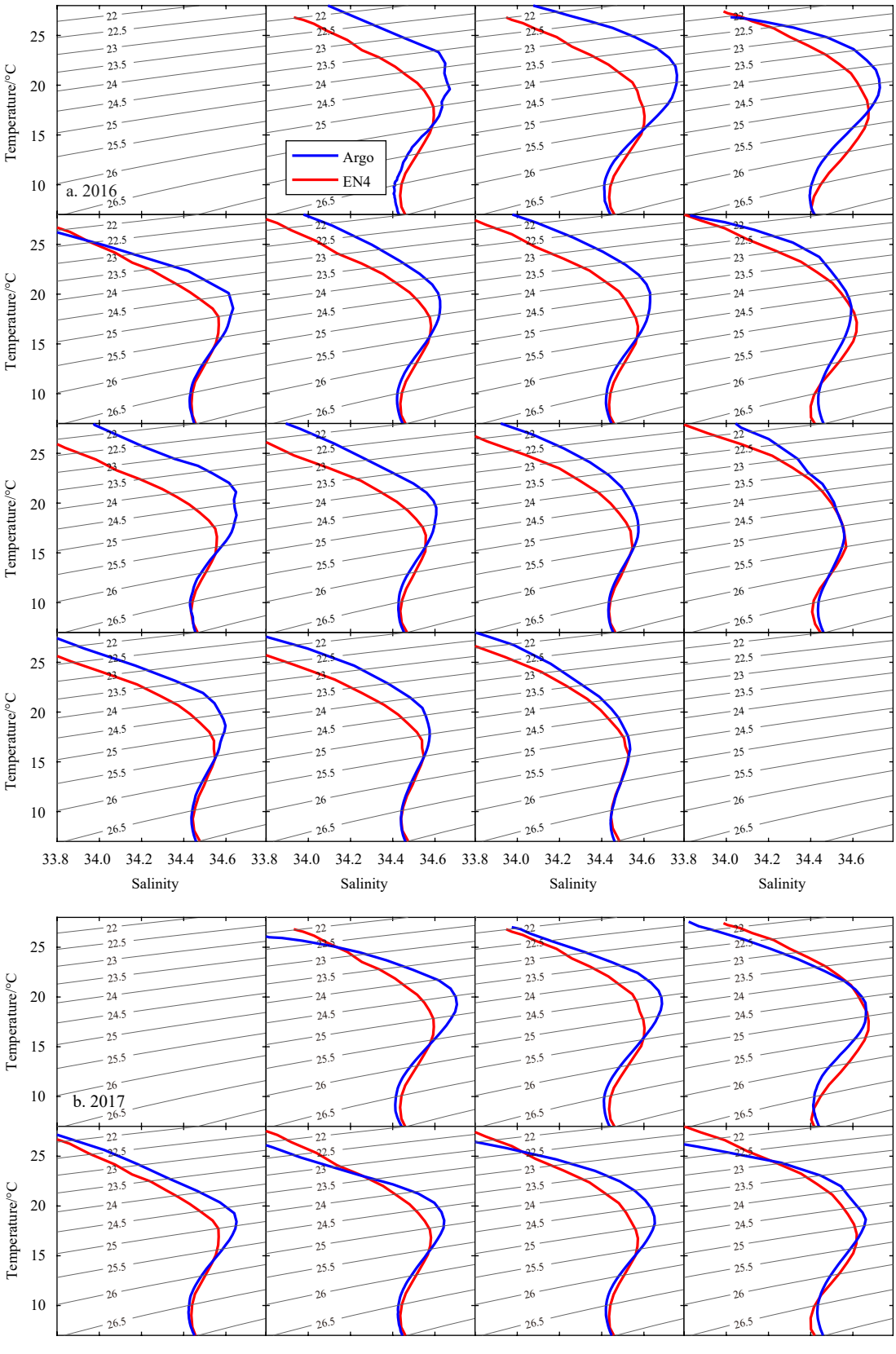


**Fig. 6.**

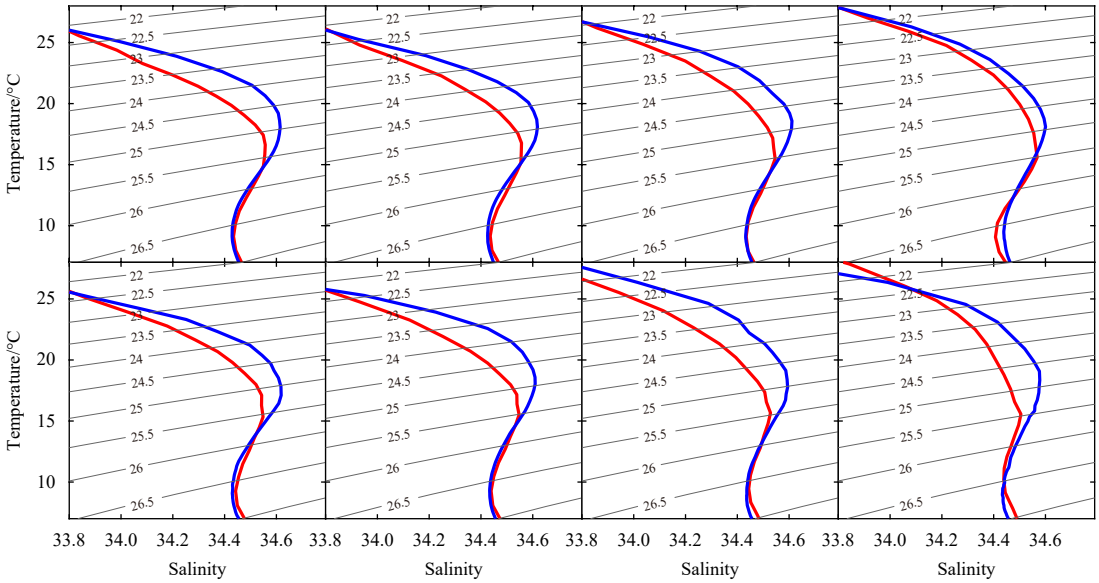


**Fig. 6.** Annual mean T–S curves in 3°×3° boxes over the South China Sea basin during 2016 (a) and 2017 (b) (Argo T–S, blue curve; EN4 climatological T–S, red curve). From left to right: 109°, 112°, 115°, 118° and 121°E; from top to bottom: 21°, 18°, 15°, 12° and 9°N.

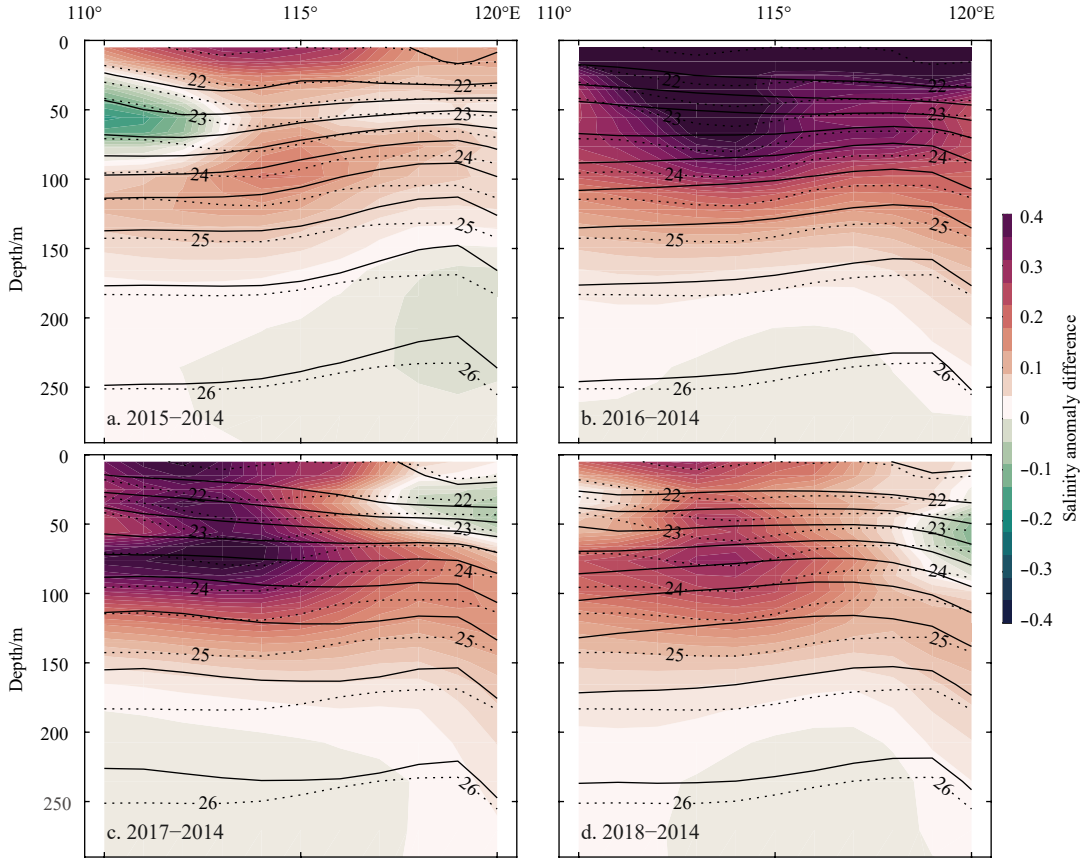


**Fig. 7.** Vertical section of differences in salinity anomalies (based on EN4 data) along 18°N between 2015 and 2014 (a), 2016 and 2014 (b), 2017 and 2014 (c), and 2018 and 2014 (d), respectively. Isopycnal contours are denoted by black solid and dotted (2014) lines.

positive wind stress curl anomalies migrated southward, reducing the trade winds in the tropical North Pacific. Thus, the NEC bifurcation shifted northward and enhanced the Kuroshio intrusion into the SCS (Yu and Qu, 2013). The results from SODA differed in magnitude from GODAS, which is probably a result of difference in the assimilation algorithm and observations used in the assimilation.

We have chosen to use only the GODAS output in the following analysis. Figure 10 shows the time series (1980–2018) of normalized SLST and subsurface salinity anomalies derived from

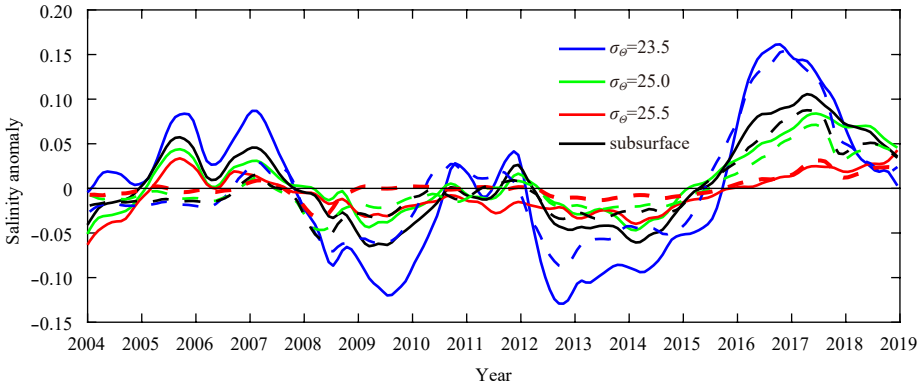


**Fig. 8.** Time series of regionally averaged salinity anomalies from 2004 to 2018 along the 23.5$\sigma_\theta$, 25$\sigma_\theta$, 25.5$\sigma_\theta$ isopycnal surfaces and entire subsurface (within the range 23.5$\sigma_\theta$–25.5$\sigma_\theta$). Solid lines denote results from EN4, and dashed lines denote results from BOA_Argo. All curves have been smoothed by a 12-month low-pass filter.

**Table 1.** Average subsurface salinity anomaly during 2016–2017 calculated from EN4 and BOA_Argo data along different isopycnal surfaces

| Isopycnal surface/kg·m$^{-3}$ | EN4 | BOA_Argo |
|---|---|---|
| 23.5–25.5$\sigma_\theta$ | 0.086 | 0.065 |
| 23.5$\sigma_\theta$ | 0.130 | 0.119 |
| 25.0$\sigma_\theta$ | 0.063 | 0.047 |
| 25.5$\sigma_\theta$ | 0.014 | 0.017 |

EN4 data within the density range of 23.5$\sigma_\theta$–25.5$\sigma_\theta$ isopycnal surfaces in the whole SCS. There was a clear positive trend of SLST into the SCS, which began at the end of 2013 and peaked in early 2016. Mean subsurface transport increased from 2.7×10$^6$ m$^3$/s to 5.1×10$^6$ m$^3$/s, and then decreased to 3.9×10$^6$ m$^3$/s by the end of 2017 (not shown). From 2014 to 2017, SLST exhibited a semiannual lead ahead of subsurface salinity changes. Interannual variation in subsurface salinity changes in the whole SCS is correlated with SLST with a 6-month lag correlation coefficient of ~0.34, which is significant at the 95% confidence level (Fig. 10). This indicates that the interannual subsurface salinity changes in the SCS were significantly influenced by the strength of the Kuroshio intrusion through the Luzon Strait.

### 4.2 *Influence of local wind stress curl*

Previous studies (Zeng et al., 2016; Nan et al., 2016) have revealed that horizontal advection and vertical entrainment are key

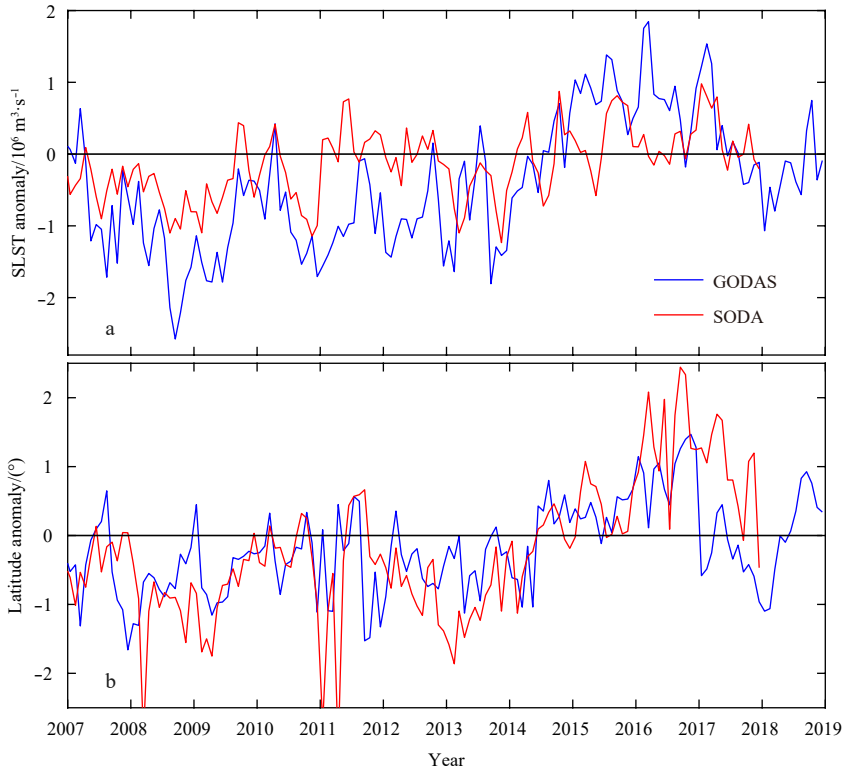


**Fig. 9.** Time series of the subsurface Luzon Strait transport (SLST) anomaly (with seasonal cycle removed) along 121°E (a) and the subsurface bifurcation latitude of the North Equatorial Current anomaly (with seasonal cycle removed) (b) based on Global Ocean Data Assimilation System (GODAS) and Simple Ocean Data Assimilation ocean/sea ice reanalysis (SODA 3.4.2), respectively.

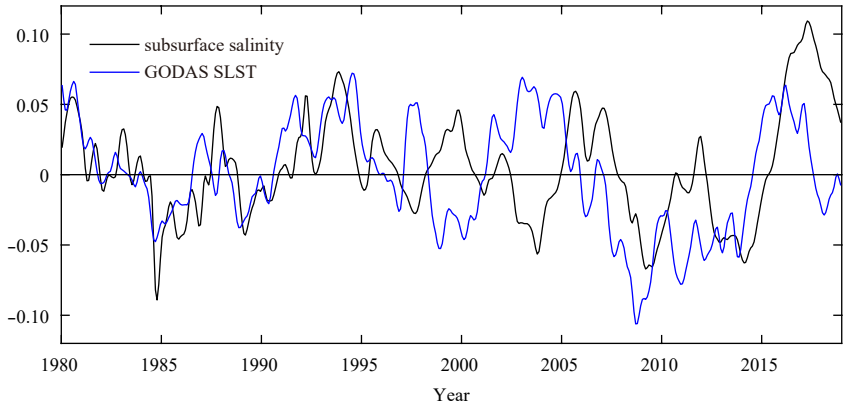


**Fig. 10.** Low-pass filtered time series (1980–2018) of the normalized SLST based on GODAS data and salinity anomaly within the range 23.5$\sigma_\theta$–25.5$\sigma_\theta$. Seasonal signals have been removed from both SLST and salinity data.

factors controlling changes in subsurface salinity. The former is favorable for subsurface salinification, and the latter is the source of subsurface freshening. Figure 11 shows the annual mean wind stress curl anomalies in the SCS from 2013 to 2018. A positive (negative) wind stress curl anomaly was found to be in the northern (southern) SCS during 2013–2014. The positive anomaly extended to the Vietnamese coast along the South China continental shelf and slope during 2015–2016 and reached its largest coverage in 2016, whereas the central basin was occupied by an enhanced negative wind stress curl anomaly. After 2016, the positive anomaly along the South China continental shelf and slope reversed, whereas the Vietnamese coast was still occupied by this positive wind stress curl anomaly. In general, a positive trend was found along the South China continental shelf and slope and the western boundary along the Vietnamese coast with a maximum rate of increase exceeding $2\times10^{-8}$ N/(m$^3$·a) to the southeast of Vietnam (not shown). To the southeast of this region is an area of depressed wind stress curl. An increase in wind stress curl usually enhances vertical entrainment from wind-driven upwelling (Yan et al., 2015; Pei et al., 2017). However, along the western boundary of the SCS, horizontal advection driven by LST was predominant, resulting in salinification, whereas in other parts of the SCS, particularly in the south, vertical entrainment was inhibited, favoring the preservation of subsurface high salinity characteristics.

## 5 Summary and discussion

A significant salinification trend in the upper layer of the SCS starting from late 2012 was reported by Zeng et al., (2018). Despite this, how salinity changes in the subsurface of the SCS in recent years had not been reported yet. Using Argo and underwater glider temperature and salinity observations, we confirmed this salinification trend in the subsurface (23.5$\sigma_\theta$–25.5$\sigma_\theta$) of the whole SCS basin started from late 2012 and reached its peak during 2016–2017. The salinification trend weakened from 2018. Subsurface water with salinity maxima exceeding 35 had never been reported previously, but this was observed by three Argo floats in the northeastern SCS during 2015–2016. Subsequently, EN4 objective analyses and BOA_Argo gridded data were used to quantitatively examine this recent increase in salinity.

The salinity increase in subsurface started in the northeastern SCS and extended southwestward gradually; the salinity maxima during 2016–2017 sometimes exceeded 0.2. The largest increase was found along the 23.5$\sigma_\theta$ isopycnal surface. Using EN4 data, we found a salinification of 0.014–0.130 along the 25.5$\sigma_\theta$–23.5$\sigma_\theta$is opycnal surfaces during 2016–2017, compared with the

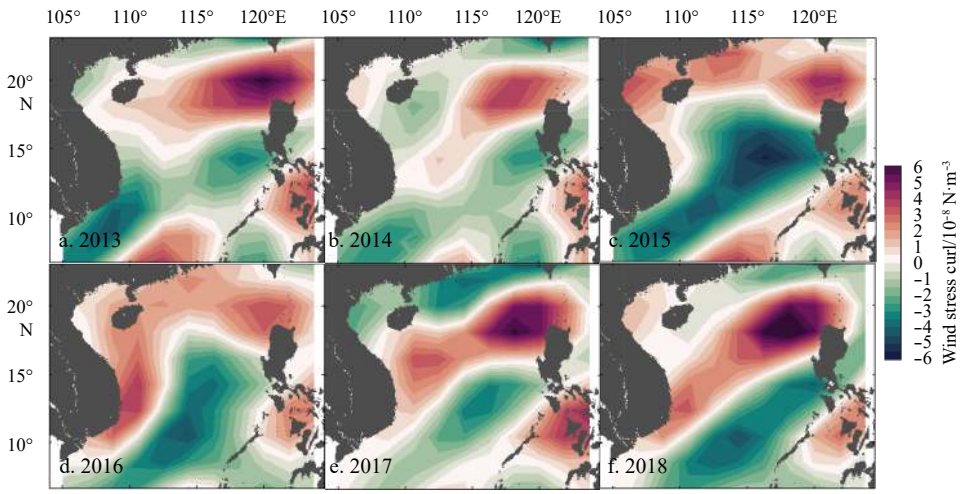


**Fig. 11.** Annual mean wind stress curl anomalies derived from the National Centers for Environmental Prediction (NCEP) monthly reanalysis.

monthly climatology. The vertical section along 18°N also exhibited a significant salinity increase that peaked in 2016. It is worth noting that the isopycnal contours along 18°N were uplifted particularly during 2017, indicating strengthened upwelling from local wind stress curl (Fig. 11). Though the accuracy of salinity from EN4 and BOA_Argo cannot be estimated accurately, both data sets are based on observation, and their time series of regionally averaged subsurface salinity anomalies in the SCS agree with each other (Fig. 8). Thus the salinity data from both EN4 and BOA_Argo are reliable to a certain degree.

Because horizontal advection and vertical entrainment are key factors controlling changes in subsurface salinity, both SLST from GODAS model output and local wind stress curl derived from NCEP reanalysis were analyzed. The results revealed that following a weakening of the Kuroshio intrusion over 1993–2012, SLST started to increase at the end of 2013 at an annual rate of ~$0.538\times10^6$ $m^3/s$. Interannual variation of SLST was correlated with salinity changes in the subsurface. Over the whole SCS basin, the correlation coefficient between salinity changes and SLST in the subsurface was up to ~0.34 with a 6-month lag. Analyses of the local wind stress curl mainly indicated a positive trend in the northern SCS and a negative trend in the southern SCS over the period 2014–2017. The positive trend reached its highest spatial coverage in 2016, spanning the western boundary from Taiwan Island to the Vietnamese coast, and favored vertical entrainment. However, advection driven by SLST was predominant along the western boundary of the SCS, which resulted in a significant salinity increase during 2016 when the SLST was highest.

In summary, this study reported an extreme salinification events in the SCS subsurface from during 2016–2017, and possible factors controlling this change were discussed. However, many associated factors concerning the observed salinification, such as details about its dynamic mechanism, relationship with the extreme El Niño event during 2015–2016, switches in the PDO from negative to positive phases, as well as its impact on ocean circulation in the SCS and possible duration, require further investigation.

The lack of long-term observations has limited our understanding of the variability in the thermohaline structure over the entire SCS. Although Argo deployment in the SCS started in 2006, the number of operational floats has never been sufficient to monitor the whole basin and construct monthly gridded fields. The Argo program has suggested that at least 22 operational floats should be maintained in the SCS. In recent years, underwater gliders have been adopted to monitor meso-scale eddies in the northern SCS; however, they are usually not routinely operated. Currently, Argo floats and underwater gliders are the most two efficient means to obtain temperature and salinity profiles on a large spatio-temporal scale, with the aims of observing different ocean phenomena. It is therefore critical to conduct multi-platform four-dimensional observational surveys with Argo floats and gliders in the SCS, focusing on the northern region where the water masses are evidently influenced by the western Pacific through the Luzon Strait.

***Acknowledgments***

This work benefited from numerous data sets that were freely available. The Argo data were collected and made freely available by the International Argo Program and the national programs that contribute to it (http://www.argo.ucsd.edu, http://argo.jcommops.org). The Argo Program is part of the Global Ocean Observing System (http://doi.org/10.17882/42182). All the Argo T/S profiles have been post-quality controlled by the China Argo Real-time Data Center (http://www.argo.org.cn); the Sea-wing underwater glider data are provided by the State Key Laboratory of Robotics, Shenyang Institute of Automation, Chinese Academy of Sciences. The BOA_Argo gridded data set was developed and provided by the China Argo Real-time Data Center. The EN4.2.1 monthly data set were produced by the UK Met Office Hadley Centre for Climate Change and made freely available at https://www.metoffice.gov.uk/hadobs/en4/. The GODAS model outputs were downloaded from http://www.esrl.noaa.gov/psd/data/gridded/data.godas.html, and the SODA 3.4.2 outputs were from https://www.atmos.umd.edu/~ocean/index_files/soda3.4.2_mn_download.htm. The monthly sea surface wind reanalysis was produced by the U.S. NCEP/NCAR and made available at http://www.esrl.noaa.gov/psd/data/gridded/data.ncep.reanalysis.derived.surface.html. We thank Tina Tin and Kara Bogus from Liwen Bianji, Edanz Group China (www.liwenbianji.cn/ac), for editing the English text of a draft of this manuscript.

**References**

Argo Science Team. 1998. On the design and implementation of Argo: an initial plan for a global array of profiling floats. Melbourne: GODAE International Project Office

Behringer D W, Ji Ming, Leetmaa A. 1998. An improved coupled model for ENSO prediction and implications for ocean initialization. Part I: the ocean data assimilation system. Monthly Weather Review, 126(4): 1013–1021, doi: 10.1175/1520-0493(1998)126<1013:AICMFE>2.0.CO;2

Behringer D W, Xue Y. 2004. Evaluation of the global ocean data assimilation system at NCEP: the Pacific Ocean. In: Proceedings of the 8th Symposium on Integrated Observing and Assimilation System for Atmosphere, Ocean, and Land Surface, AMS 84th Annual Meeting. Seattle, Washington: Washington State Convention and Trade Center, 11–15

Boyer T P, Levitus S, Antonov J I, et al. 2005. Linear trends in salinity for the world ocean, 1955–1998. Geophysical Research Letters, 32(1): L01604

Carton J A, Chepurin G A, Chen Ligang. 2018. SODA3: a new ocean climate reanalysis. Journal of Climate, 31(17): 6967–6983, doi: 10.1175/JCLI-D-18-0149.1

Curry R, Dickson B, Yashayaev I. 2003. A change in the freshwater balance of the Atlantic Ocean over the past four decades. Nature, 426(6968): 826–829, doi: 10.1038/nature02206

Delcroix T, Cravatte S, McPhaden M J. 2007. Decadal variations and trends in tropical Pacific sea surface salinity since 1970. Journal of Geophysical Research: Oceans, 112(C3): C03012

Durack P J, Wijffels S E. 2010. Fifty-year trends in global ocean salinities and their relationship to broad-scale warming. Journal of Climate, 23(16): 4342–4362, doi: 10.1175/2010JCLI3377.1

Good S A, Martin M J, Rayner N A. 2013. EN4: quality controlled ocean temperature and salinity profiles and monthly objective analyses with uncertainty estimates. Journal of Geophysical Research: Oceans, 118(12): 6704–6716, doi: 10.1002/2013JC009067

Hsin Y C. 2015. Multidecadal variations of the surface Kuroshio between 1950s and 2000s and its impacts on surrounding waters. Journal of Geophysical Research: Oceans, 120(3): 1792–1808, doi: 10.1002/2014JC010582

Jacobs S S, Giulivi C F, Mele P A. 2002. Freshening of the Ross Sea during the late 20th century. Science, 297(5580): 386–389, doi: 10.1126/science.1069574

Kalnay E, Kanamitsu M, Kistler R, et al. 1996. The NCEP/NCAR 40-year reanalysis project. Bulletin of the American Meteorological Society, 77(3): 437–472, doi: 10.1175/1520-0477(1996)077<0437:TNYRP>2.0.CO;2

Li Li, Qu Tangdong. 2006. Thermohaline circulation in the deep South China Sea basin inferred from oxygen distributions. Journal of Geophysical Research: Oceans, 111(C5): C05017

Li Li, Wu Risheng, Guo Xiaogang. 2000. Seasonal circulation in the South China Sea—a TOPEX/POSEIDON satellite altimetry study. Haiyang Xuebao (in Chinese), 22(6): 13–26

Li Hong, Xu Fanghua, Zhou Wei, et al. 2017. Development of a global gridded Argo data set with Barnes successive corrections. Journal of Geophysical Research: Oceans, 122(2): 866–889, doi: 10.1002/2016JC012285

Liu Zenghong, Wu Xiaofen, Xu Jianping, et al. 2017. China Argo project: progress in China Argo ocean observations and data applications. Acta Oceanologica Sinica, 36(6): 1–11, doi: 10.1007/s13131-017-1035-x

Liu Zenghong, Xu Jianping, Yu Jiancheng. 2019. Real-time Quality Control of data from Sea-Wing underwater glider installed with Glider Payload CTD sensor. Acta Oceanologica Sinica, : doi: 10.1007/s13131-019-1489-0

Lu Shaolei, Liu Zenghong, Li Hong, et al. 2019. Manual of global ocean Argo gridded data set (BOA_Argo) (Version 2019). ftp://data.argo.org.cn/pub/ARGO/BOA_Argo/doc/BOA_Argo_readme_CN_2019.pdf[2019-07-08/2019-07-15]

Lukas R. 2001. Freshening of the upper thermocline in the North Pacific subtropical gyre associated with decadal changes of rainfall. Geophysical Research Letters, 28(18): 3485–3488, doi: 10.1029/2001GL013116

Nan Feng, Xue Huijie, Chai Fei, et al. 2013. Weakening of the Kuroshio intrusion into the South China Sea over the past two decades. Journal of Climate, 26(20): 8097–8110, doi: 10.1175/JCLI-D-12-00315.1

Nan Feng, Yu Fei, Xue Huijie, et al. 2016. Freshening of the upper ocean in the South China Sea since the early 1990s. Deep Sea Research Part I: Oceanographic Research Papers, 118: 20–29, doi: 10.1016/j.dsr.2016.10.010

Pei Yuhua, Liu Xiaohui, He HaiLun. 2017. Interpreting the sea surface temperature warming trend in the Yellow Sea and East China Sea. Science China Earth Sciences, 60(8): 1558–1568, doi: 10.1007/s11430-017-9054-5

Qu Tangdong. 2000. Upper-layer circulation in the South China Sea. Journal of Physical Oceanography, 30(6): 1450–1460, doi: 10.1175/1520-0485(2000)030<1450:ULCITS>2.0.CO;2

Qu Tangdong, Kim Y Y, Yaremchuk M. 2004. Can Luzon Strait transport play a role in conveying the impact of ENSO to the South China Sea? Journal of Climate, 17(18): 3644–3657, doi: 10.1175/1520-0442(2004)017<3644:CLSTPA>2.0.CO;2

Qu Tangdong, Lukas R. 2003. The bifurcation of the North Equatorial current in the Pacific. Journal of Physical Oceanography, 33(1): 5–18, doi: 10.1175/1520-0485(2003)033<0005:TBOTNE>2.0.CO;2

Qu Tangdong, Mitsudera H, Yamagata T. 2000. Intrusion of the North Pacific waters into the South China Sea. Journal of Geophysical Research: Oceans, 105(C3): 6415–6424, doi: 10.1029/1999JC900323

Riser S C, Freeland H J, Roemmich D, et al. 2016. Fifteen years of ocean observations with the global Argo array. Nature Climate Change, 6(2): 145–153, doi: 10.1038/nclimate2872

Shaw P T. 1991. The seasonal variation of the intrusion of the Philippine sea water into the South China Sea. Journal of Geophysical Research: Oceans, 96(C1): 821–827, doi: 10.1029/90JC02367

Shaw P T, Chao S Y. 1994. Surface circulation in the South China Sea. Deep Sea Research Part I: Oceanographic Research Papers, 41(11–12): 1663–1683, doi: 10.1016/0967-0637(94)90067-1

Suga T, Kato A, Hanawa K. 2000. North Pacific tropical water: its climatology and temporal changes associated with the climate regime shift in the 1970s. Progress in Oceanography, 47(2–4): 223–256, doi: 10.1016/S0079-6611(00)00037-9

Toole J M, Millard R C, Wang Z, et al. 1990. Observations of the Pacific North Equatorial current bifurcation at the Philippine coast. Journal of Physical Oceanography, 20(2): 307–318, doi: 10.1175/1520-0485(1990)020<0307:OOTPNE>2.0.CO;2

Tsui I F, Wu C R. 2012. Variability analysis of Kuroshio intrusion through Luzon Strait using growing hierarchical self-organizing map. Ocean Dynamics, 62(8): 1187–1194, doi: 10.1007/s10236-012-0558-0

Wang Dongxiao, Xiao Jingen, Shu Yeqiang, et al. 2016. Progress on deep circulation and meridional overturning circulation in the South China Sea. Science China Earth Sciences, 59(9): 1827–1833, doi: 10.1007/s11430-016-5324-6

Wong A P S, Bindoff N L, Church J A. 1999. Large-scale freshening of intermediate waters in the Pacific and Indian oceans. Nature, 400(6743): 440–443, doi: 10.1038/22733

Wong A P S, Bindoff N L, Church J A. 2001. Freshwater and heat changes in the North and South Pacific Oceans between the 1960s and 1985-94. Journal of Climate, 14(7): 1613–1633, doi: 10.1175/1520-0442(2001)014<1613:FAHCIT>2.0.CO;2

Yan Yunwei, Ling Zheng, Chen Changlin. 2015. Winter coastal upwelling off northwest Borneo in the South China Sea. Acta Oceanologica Sinica, 34(1): 3–10, doi: 10.1007/s13131-015-0590-2

Yu Kai, Qu Tangdong. 2013. Imprint of the Pacific decadal oscillation on the South China Sea throughflow variability. Journal of Climate, 26(24): 9797–9805, doi: 10.1175/JCLI-D-12-00785.1

Yu Jiancheng, Zhang Aiqun, Jin Wenming, et al. 2011. Development and experiments of the Sea-Wing underwater glider. China Ocean Engineering, 25(4): 721–736, doi: 10.1007/s13344-011-0058-x

Yuan Yaochu, Liao Guanghong, Yang Chenghao, et al. 2014. Summer Kuroshio Intrusion through the Luzon Strait confirmed from observations and a diagnostic model in summer 2009. Progress in Oceanography, 121: 44–59, doi: 10.1016/j.pocean.2013.10.003

Zeng Lili, Chassignet E P, Schmitt R W, et al. 2018. Salinification in the South China Sea since late 2012: a reversal of the freshening since the 1990s. Geophysical Research Letters, 45(6): 2744–2751, doi: 10.1002/2017GL076574

Zeng Lili, Liu W T, Xue Huijie, et al. 2014. Freshening in the South China Sea during 2012 revealed by Aquarius and in situ data. Journal of Geophysical Research: Oceans, 119(12): 8296–8314, doi: 10.1002/2014JC010108

Zeng Lili, Wang Dongxiao, Xiu Peng, et al. 2016. Decadal variation and trends in subsurface salinity from 1960 to 2012 in the northern South China Sea. Geophysical Research Letters, 43(23): 12181–12189, doi: 10.1002/2016GL071439